Self-gated self-supervised ADMM unrolling enables mesoscale high-resolution motion-robust diffusion-weighted imaging

Zhengguo Tan, Patrick A Liebig, Annika Hofmann, Michael Jaroszewicz, Yun Jiang, Vikas Gulani, Frederik B Laun, Florian Knoll

SYNOPSIS & IMPACT

Motivation: High-resolution and motion-robust diffusion-weighted imaging (DWI) is clinically demanding. A self-supervised image reconstruction model that leverages spatial-diffusion complementary sampling and convolution is beneficial to high-quality clinical DWI.

Goal: To develop an efficient self-supervised algorithm unrolling technique for high-resolution and motion-robust DWI.

Approach: We unroll the alternating direction method of multipliers (ADMM) to perform scan-specific self-supervised learning for deep DWI reconstruction.

Results: We demonstrate that (1) ADMM unrolling is generalizable across slices, (2) ADMM unrolling outperforms compressed sensing with locally-low rank (LLR) regularization in terms of image sharpness, tissue continuity and motion robustness, (3) ADMM unrolling enables clinically feasible inference time.

Impact: Our proposed ADMM unrolling enables whole brain DWI of 21 volumes at 0.7 mm isotropic resolution and 10 minutes scan, and shows higher signal-to-noise ratio (SNR), clearer tissue delineation, and improved motion robustness, which make it plausible for clinical translation.

INTRODUCTION

The contribution of this work includes:

- We unroll the alternating direction method of multipliers (ADMM) [1] to perform self-gated scan-specific self-supervised learning for deep DWI.
- We demonstrate the generalizability of the trained ADMM unrolling model, i.e. the model trained on one single slice is applicable to other "unseen" slices. This feature, compared to slice-by-slice training, significantly reduces the training time.
- We achieve whole-brain 0.7mm DWI with 21 diffusion-encoding directions at 10 minutes scan time.

METHODS

Data Acquisition

Three volunteers and one patient with written informed consent approved by the local ethics committee participated in this study.

Brain DWI at 7T

Three volunteers were scanned at 7T (MAGNETOM Terra, Siemens, Erlangen, Germany) with the mesoscale high-resolution DWI protocol based on NAViEPI [2]: FOV 200 mm, matrix size 286 x 286 x 176, 3-shot interleaved EPI with 2x2-fold acceleration and 5/8 partial Fourier, bandwidth 972 Hz/pixel, TR/TE/ESP 8900/58/1.17 ms, and a total scan time of 10 minutes for 21 volumes (1 non-diffusion-weighted and 20 diffusion-encoded with b-value 1000 s/mm ^{2}). The total scan time is 17 minutes with navigators and 10 minutes without navigators.

Prostate DWI at 3T

One patient was scanned at 3T (MAGNETOM Vida) with the clinical prostate DWI protocol utilizing single-shot EPI: FOV 200 mm, matrix size 171 x 114 x 35, voxel size 1.75 x 1.75 x 4 mm ^{3}, 2-fold in-plane acceleration, TR/TE 6400/91 ms, and the 3-scan trace mode with b-values 0, 100, 800, and 1600 s/mm ^{2} and 97 volumes. ADC was obtained as the average of diagonal tensors, which was fitted from diffusion-weighted images excluding the b-value 1600 s/mm ^{2}.

Forward Modeling and Reconstruction

Joint k-q-slice reconstruction [2] formulates the forward model as,

$$\mathcal{A}(\mathbf{x}) = \mathbf{P \Sigma \Theta F S \Phi} \mathbf{x}$$

The multi-band multi-diffusion-weighted images ($\mathbf{x}$) is mapped to k-space via a chain of linear operators, including the shot-to-shot phase variation ($\mathbf{\Phi}$), coil sensitivities ($\mathbf{S}$), 2D FFT ($\mathbf{F}$), multi-band phases ($\mathbf{\Sigma\Theta}$), and the undersampling mask ($\mathbf{P}$). The shot phase can be estimated from either the navigator echo or the imaging echo (self-gated). With the forward model ($\mathcal{A}$), the joint reconstruction reads,

$$\text{argmin}_{\mathbf{x}} \left\lVert \mathbf{y} - \mathcal{A}(\mathbf{x}) \right\rVert _2^2 + \lambda \mathcal{R}(\mathbf{x})$$

$\mathbf{y}$ is the measured k-space. The regularization $\mathcal{R}(\mathbf{x})$ is either nuclear norms of the local spatial-diffusion patches for LLR-regularized reconstruction or the 2D ResNet [3] for unrolled reconstruction. In both cases, we employ ADMM to assure fair comparison.

Self-Gated Self-Supervised ADMM Unrolling

a) uniform spliting

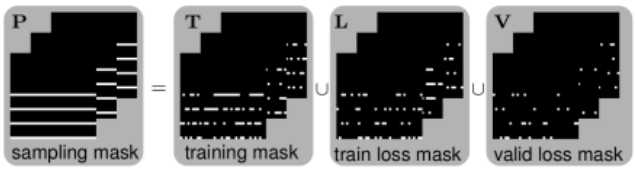

b) ADMM with ResNet

$$\begin{cases} \mathbf{x}^{(k+1)} = \underset{\mathbf{x}^{(k)}}{\operatorname{argmin}} \left\| \mathbf{y} - \mathcal{A}(\mathbf{x}^{(k)}) \right\|_2^2 + \frac{\rho}{2} \left\| \mathbf{x}^{(k)} - \mathbf{v}^{(k)} + \mathbf{u}^{(k)} \right\|_2^2 \\ \mathbf{v}^{(k+1)} = (\lambda/\rho) \cdot \mathcal{D}_\omega(\mathbf{x}^{(k+1)} + \mathbf{u}^{(k)}) \\ \mathbf{u}^{(k+1)} = \mathbf{u}^{(k)} + \mathbf{x}^{(k+1)} - \mathbf{v}^{(k+1)} \end{cases}$$

c) ADMM unrolling training

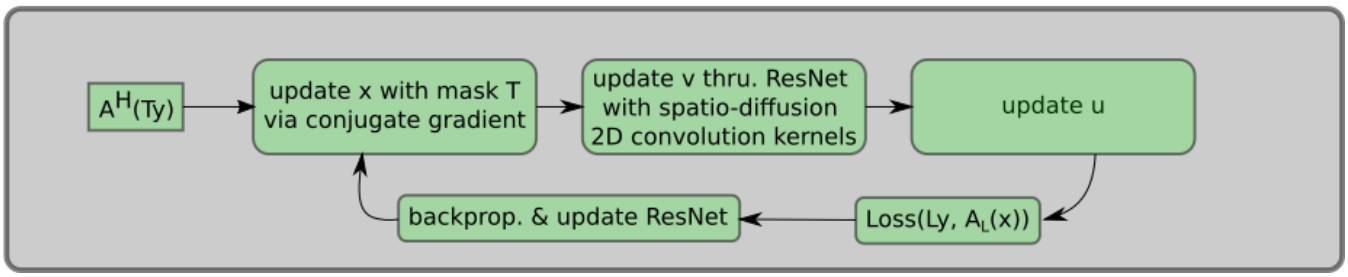

> **Figure 1.** Key components in ADMM unrolling. (a) The sampling mask P was uniformly split into three disjoint sets: the training mask T for the data consistency term during training, the train loss mask L for the loss function calculation during training, and the validation loss mask V for the loss function calculation during validation. (b) ADMM update rules. (c) The flowchart for the training procedure. The ResNet parameters are updated via ADAM during training, but remain fixed during validation.

Inspired by Yaman et al. [4], our proposed ADMM unrolling is scan specific, i.e., the model is trained on one single dataset. The data sampling mask $\mathbf{P}$ in Figure 1 is split into three disjoint sets. Each set consists of 12 repetitions constructed via random uniform sampling of the data mask $\mathbf{P}$. In each training epoch, every repetition is looped through utilizing ADMM with the training mask $\mathbf{T}$ and the training loss mask $\mathbf{L}$ to update the ResNet parameters ω. The validation loss is computed after every training epoch to update the minimal validation loss, which, if not reduced for 12 consecutive epochs, terminates the training. The 2D convolution in ResNet is performed in the spatial-diffusion dimension, with the diffusion encoding as the convolution channel. All reconstructions were done on a A100 SXM4/NVLink GPU with 80GB memory (NVIDIA, Santa Clara, CA, USA).

RESULTS AND DISCUSSION

Figures 2-4 are gif movies displayed at 1.5 seconds/frame.

Model Generalizability

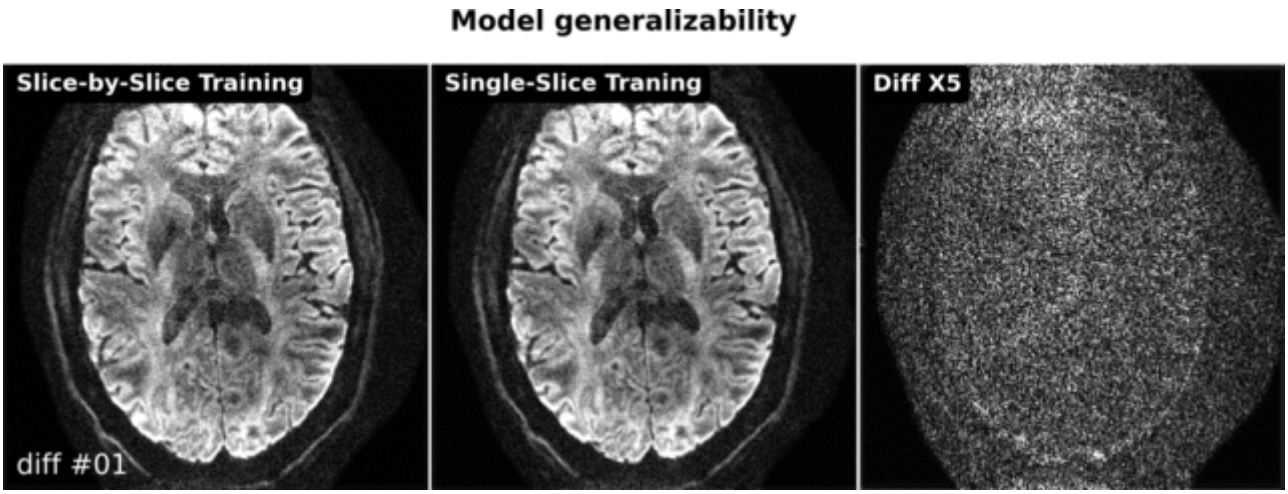

> **Figure 2.** Comparison of two training strategies: (1) slice-by-slice training, where every slice is trained and tested individually; (2) single-slice training, where the unrolled ADMM model is trained on only one slice and tested on all remaining slices. No major qualitative or quantitative difference can be seen between the two training strategies.

Figure 2 demonstrates the generalizability of ADMM unrolling, i.e., an unrolled ADMM model trained on one single slice is applicable to all remaining "unseen" slices. The absolute difference along all diffusion encoding show no major difference.

Self-Gated Self-Supervised ADMM Unrolling

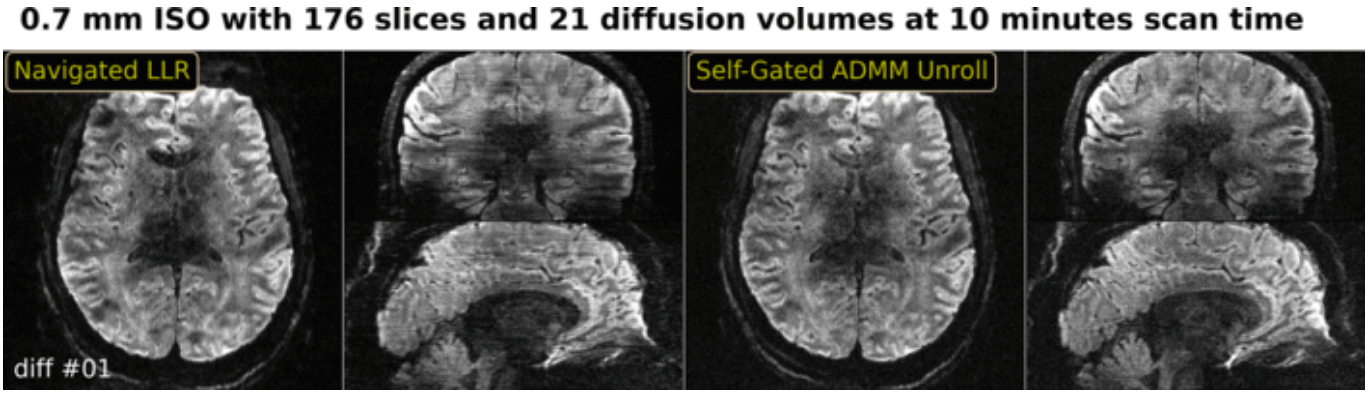

> **Figure 3.** Comparison of (left) navigated LLR and (right) self-gated ADMM unrolling reconstruction on 0.7mm isotropic resolution DWI. The use of navigators prolongs the total scan time, and thus increases the sensitivity to motion, as shown in navigated reconstruction. The retrospectively self-gated reconstruction discards navigators, and renders sharper diffusion-weighted images. Compared to LLR, unrolled ADMM is advantageous in resolving clearer tissue boundaries in diffusion-weighted images.

Figures 3 demonstrates the efficacy of the self-gated self-supervised ADMM unrolling reconstruction. The use of navigators come with the drawbacks of elongated acquisition and higher motion sensitivity, which may result in ghosting (axial) and striping (coronal and sagittal) artifacts, such as the 5th diffusion encoding in the navigated LLR reconstruction.

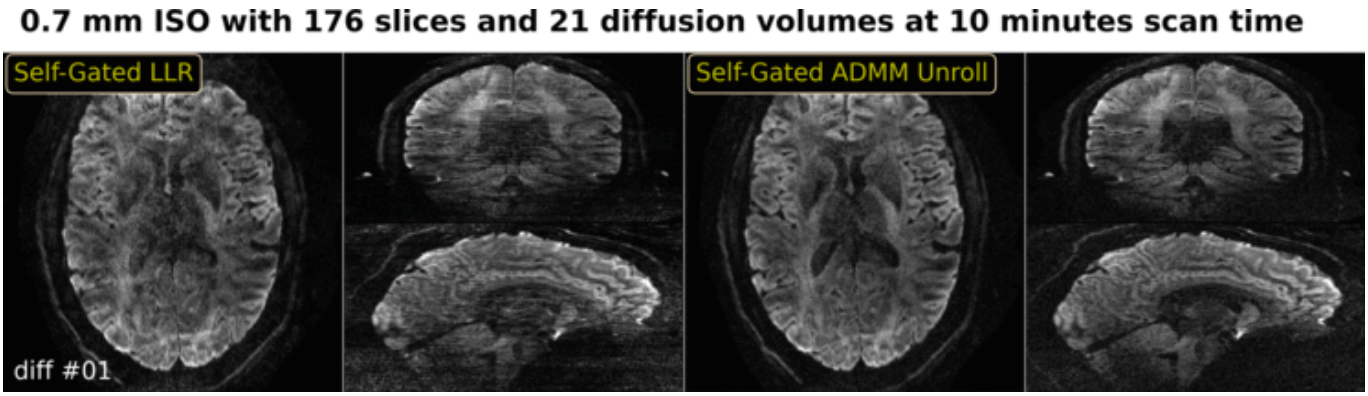

> **Figure 4.** Comparison of prospectively self-gated (left) LLR and (right) ADMM unrolling reconstruction on 0.7mm isotropic resolution DWI. ADMM unrolling reduces phase ambiguities in the shot-combined reconstruction, thereby rendering clearer tissue delineation and reducing stripping artifacts.

Figure 4 shows the reconstruction results from an non-navigated acquisition. ADMM unrolling illustrates much reduced axial blurring and sagittal/coronal striping artifacts than LLR. In addition, the inference of every slice takes only about one minute, whereas the implemented LLR reconstruction takes about 48 minutes per slice.

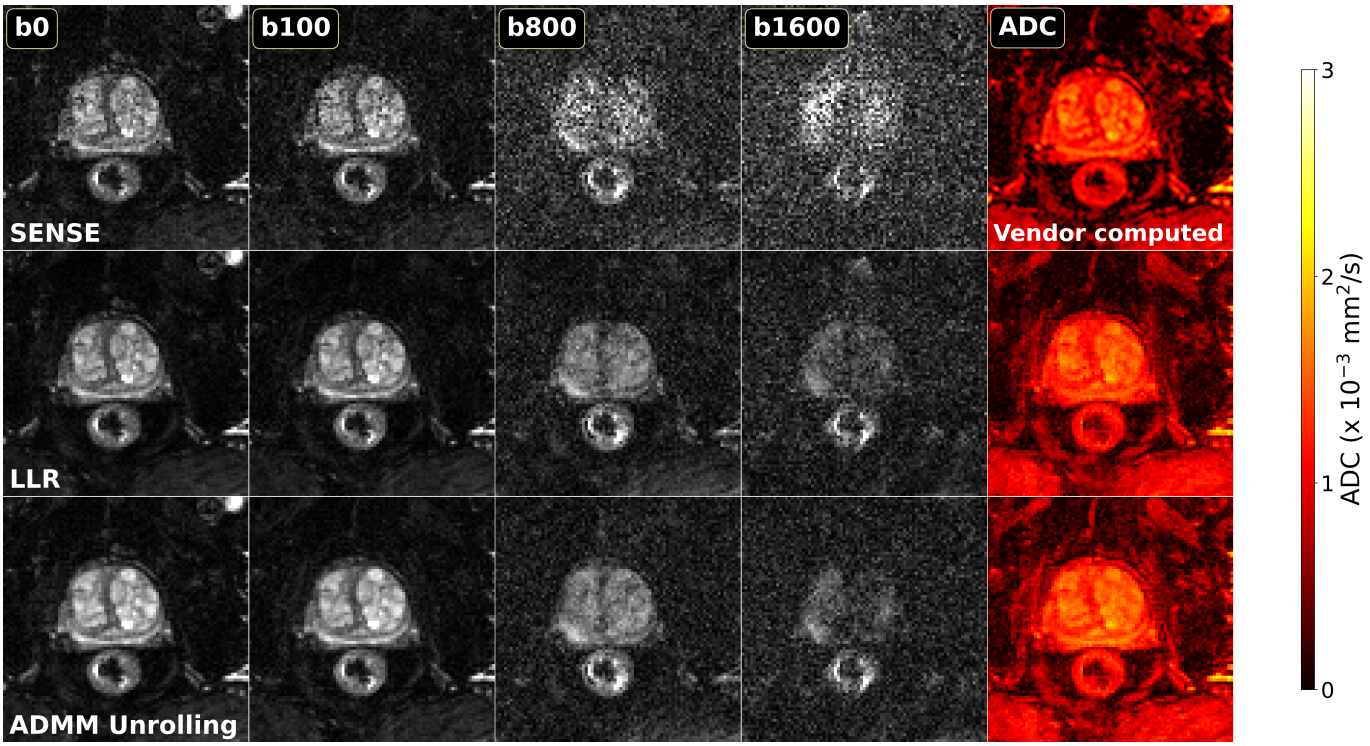

Figure 5. Comparison of reconstructions for prostate DWI: (top) parallel imaging as SENSE, (middle) compressed sensing with LLR regularization, and (bottom) ADMM unrolling. b0, diffusion-weighted images at different b-values, and ADC maps are displayed from left to right. The ADC map in the top row was supplied by Vendor online reconstruction, whereas the others were fitted directly from reconstructed diffusion-weighted images in MRtrix3 (https://www.mrtrix.org/). Both LLR and ADMM unrolling show strong denoising capabilities.

Figure 5 shows preliminary results on prostate DWI reconstruction. While the clinical portocol with online reconstruction may have internal filtering, our ADC maps were fitted directly from reconstructed diffusion-weighted images. ADMM unrolling shows strong denoising and renders clear tissue delineation.

CONCLUSION

We proposed a self-gated self-supervised learning reconstruction for high-resolution and motion-robust DWI. Based on the mechanism of data split (cross validation), our proposed ADMM unrolling requires only one slice for training and is generalized cross-slice. Our method has been validated in both neuro and prostate DWI.

REFERENCES

[1] Boyd S, Parikh N, Chu E, Peleato B, Eckstein J. Distributed optimization and statistical learning via the althernating direction method of multipliers. Foundations and Trends in Machine Learning 2010;3:1-122.

[2] Tan Z, Liebig PA, Heidemann RM, Laun FB, Knoll F. Accelerated diffusion-weighted magnetic resonance imaging at 7 T: Joint reconstruction for shift-encoded navigator-based interleaved echo planar imaging (JETS-NAViEPI). Imaging Neuroscience 2024;2:1-15.

[3] He K, Zhang X, Ren S, Sun J. Deep residual learning for image recognition. in IEEE Conference on Computer Vision and Pattern Recognition (CVPR'16). 2016:770-778.

[4] Yaman B, Hosseini SAH, Akçakaya M. Zero-shot self-supervised learning for MRI reconstruction. in 10th International Conference on Learning Representations (ICLR'10). 2022.